Tokamak ITG-KBM transition benchmarking with the mixed variables/pullback transformation electromagnetic gyrokinetic scheme

M. D. J. Cole,[1, a)] A. Mishchenko,[2] A. Bottino,[3] and C. S. Chang[1]
[1)] *Princeton Plasma Physics Laboratory, Princeton University, Princeton, New Jersey 08543, USA*
[2)] *Max Planck Institute for Plasma Physics, D-17491 Greifswald, Germany*
[3)] *Max Planck Institute for Plasma Physics, D-85748 Garching, Germany*

(Dated: 30 January 2021)

Electromagnetic gyrokinetic simulation of high temperature plasma is required to predict confinement in magnetic fusion devices and has posed challenges for existing codes. In this paper, we demonstrate successful global gyrokinetic simulation of the ITG-KBM transition in a toroidal fusion plasma test case using the mixed variables/pullback transformation (MV/PT) scheme with the particle-in-cell codes XGC and ORB5, and compare to results from a conventional continuum code from the literature. The MV/PT scheme combines explicit time integration with mitigation of the well-known electromagnetic gyrokinetic 'cancellation problem.' We calculate eigenmodes in the electrostatic and parallel vector potentials, and find good agreement in growth rate, real frequency, and the normalized plasma pressure of mode transition.

Introduction Gyrokinetics is a reduced model of plasma dynamics that decouples the fast gyromotion from the slower gyrocentre motion[1]. It is valid for modelling plasma phenomena with a frequency much lower than the gyrofrequency and length scales comparable to the gyroradius. It has been widely applied for numerically to fusion plasmas. Reduced dimensionality and elimination of high frequency dynamics minimises computational cost while accurately representing dominant transport mechanisms. This means in particular turbulent transport in tokamaks and stellarators. Early work typically modelled the slower thermal ions in the electrostatic approximation, with an adiabatic approximation for the electron density response. Recently several codes model kinetic electrons and magnetic fluctuations globally to the last closed flux surface. These include ORB5[2,3], EUTERPE[4,5], GEM[6], GENE[7] and GKW[8].

XGC is a gyrokinetic code originally designed for modelling the edge region of tokamaks to the first wall[9–11]. It is also fully capable of conventional core region modelling in tokamaks and, recently, stellarators[12–14]. Most XGC simulations have been electrostatic, with adiabatic or kinetic electrons. To include fluctuations in the parallel vector potential, three approaches have been taken in XGC. One is to model electrons as a fluid, allowing the use of the electromagnetic gyrokinetic equations of motion and Ampére's law in the $v_{||}$ formulation[1,15]. Another is solving the gyrokinetic Vlasov-Maxwell system in the $v_{||}$ formulation with implicit methods to calculate the fluctuating vector potential[16]. The third, here, is to use the mixed formulation[4,17,18]. These equations can be solved explicitly, but introduce a 'cancellation problem' arising from the skin terms in Ampére's law. An accurate cancellation of the corresponding mixed variables current component is necessary, which can be large relative to the total mixed variables current.

The mixed variables/pullback transformation (MV/PT) scheme minimises these current contributions and introduces an analytical simplification in the gyrokinetic equations of motion[4]. In previous work, the implementation of this scheme in the ORB5 code has been described in detail[3]. The MV/PT scheme has now also been implemented in XGC.

Electromagnetic microturbulence is an important transport mechanism that can be modelled with a global gyrokinetic code. Microturbulence is known to be the main cause of transport in tokamaks in reactor-relevant operation. It is also known that the character of microturbulence can change substantially with finite normalised plasma pressure, $\beta = 2\mu_0 nT/B^2$, requiring an electromagnetic treatment. The toroidal branch of the ion temperature gradient-driven mode (ITG) is typically suppressed at finite β, but can become subdominant to the kinetic ballooning mode (KBM), both driven by the ion temperature gradient. An accurate treatment of this physics is needed to predict experimental transport. A linear benchmark case for this phenomenon has been performed by a number of global electromagnetic gyrokinetic codes[19]. Key quantities include the growth rates and real frequencies of the modes calculated for different normalised plasma pressure profiles, the calculated eigenmode structures, and the location of the ITG-KBM transition in terms of the normalised plasma pressure.

In previous work, the new MV/PT scheme was not used. Here, we use this case to verify the scheme using separate implementations in two gyrokinetic particle-in-cell codes, XGC and ORB5. This is also a first verification of the global electromagnetic capability of the XGC code. The XGC code has substantial numerical differences to other gyrokinetic particle-in-cell codes. Being

[a)] mcole@pppl.gov

designed for edge simulations, it uses an unstructured mesh to permit simulations through the separatrix and including X-points.

Numerical model XGC is a whole volume, total-f gyrokinetic PIC code[11]. In this paper, we use its core delta-f capability, although the MV/PT scheme is applicable for full-f simulations and is being verified for the edge region with XGC. This paper also considers only perpendicular magnetic perturbations, $\delta B_{||} = 0$. Ampére's law must now be solved to calculate $A_{||}$, and corresponding magnetic fluctuation terms newly appear in the gyrokinetic equations of motion. In the mixed formulation, the parallel vector potential is further separated into two components, $A_{||} = A_{||}^{(h)} + A_{||}^{(s)}$[17,18]. These components correspond to the total vector potential in the Hamiltonian ($p_{||}$) and symplectic ($v_{||}$) respectively, hence the superscripts h and s.

In the mixed formulation, Ampére's law with the long-wavelength approximation is

$$-\nabla^2 A_{||}^{(h)} + A_{||}^{(h)} \sum_s \frac{\mu_0 n_0 q_s^2}{m_s} = \mu_0 \sum_s \left\langle \delta j_{||,s} \right\rangle + \nabla^2 A_{||}^{(s)} \tag{1}$$

where s is the species subscript, μ_0 is the permeability of free space, n_0 the background density, q_s the species charge, m_s the species mass, $\delta j_{||}$ the perturbed mixed formulation current, and $\langle\rangle$ the gyroaverage operator. The skin terms are $\sum_s \frac{\mu_0 n_0 q_s^2}{m_s}$, where the electron skin term dominates with factor $1/m_s$. These give rise to the cancellation problem as they must cancel a large non-physical components of the MV, which is only the physical current for $A_{||}^{(h)} = 0$. The problem is mitigated by minimisation of $A_{||}^{(h)}$ as a fraction of $A_{||}$, in the MV/PT scheme by updating $A_{||}^{(s)}$ to accurately predict the evolution of $A_{||}$ and by periodic resetting via the pullback transformation.

The $A_{||}$ splitting introduces an additional degree of freedom and therefore requires an additional equation. We take advantage of this to predict $A_{||}$ by introducing a new Ohm's law-like equation for the evolution of $A_{||}^{(s)}$. Unlike in a fluid hybrid model, this does not truncate the physics, as any inaccuracy is corrected by solving Ampére's law. We use the equation,

$$\partial A_{||}^{(s)}/\partial t = -\nabla_{||}\phi. \tag{2}$$

It accurately predicts the evolution of $A_{||}$ for many modes, such as ideal kinetic-MHD modes. It also allows analytical cancellation of the often large $\nabla_{||}\phi$ term in the PIC weight evolution equation[4].

Since the division of $A_{||}$ into h and s components is arbitrary, $A_{||}^{(h)}$ can be set to zero at each timestep, provided $A_{||}^{(s)}$ and the marker weights are consistently updated (pullback). In the linear delta-f formulation, the pullback equation is,[4],

$$\delta f_s(v_{||}) = \delta f_s(u_{||}) + \frac{q_s}{m_s}\frac{\partial f_{s,0}}{\partial u_{||}}\left\langle A_{||}^{(h)} \right\rangle, \tag{3}$$

where $v_{||}$ is the symplectic ($A_{||}^{(h)} = 0$) or physical velocity, while $u_{||} = v_{||} + \frac{q_s}{m_s}\left\langle A_{||}^{(h)} \right\rangle$ is the mixed variables velocity.

The equations of motion have been recast in the $\rho_{||}$ formalism used by XGC as

$$\dot{\vec{R}} = D\left[\frac{q_s}{m_s}\left(\rho_{\|} - \frac{\langle A_{\|}^{(h)}\rangle}{B}\right)\left(\vec{B} + \left(\rho_{\|} + \frac{\langle A_{\|}^{(s)}\rangle}{B}\right)\nabla\times\vec{B} + \nabla\langle A_{\|}^{(s)}\rangle\times\vec{b}\right) + \frac{\vec{B}\times\nabla_{\rho_{\|}}H_{XGC}}{B^2}\right] \tag{4}$$

and

$$\dot{\rho}_{\|} = -\frac{1}{B}\frac{\partial\left\langle A_{\|}^{(s)}\right\rangle}{\partial t} - \frac{D}{B^2}\nabla_{\rho_{\|}}H_{XGC}\cdot\left[\vec{B} + \left(\rho_{\|} + \frac{\left\langle A_{\|}^{(s)}\right\rangle}{B}\right)\nabla\times\vec{B} + \nabla\left\langle A_{\|}^{(s)}\right\rangle\times\vec{b}\right], \tag{5}$$

where

$$\nabla H_{XGC} = \frac{\nabla B}{q_s}\left(\frac{q_s^2 B}{m_s}\rho_{\|}^2 + \mu\right) + \nabla\left\langle\phi - \frac{q_s B}{m_s}\rho_{\|}A_{\|}^{(\mathrm{h})}\right\rangle \tag{6}$$

and

$$D^{-1} = 1 + \left(\rho_{\|} + \frac{\left\langle A_{\|}^{(\mathrm{s})}\right\rangle}{B}\right)\frac{\vec{B}\cdot\nabla\times\vec{B}}{B^2}. \tag{7}$$

In these equations, $\rho_{||} = \frac{m_s v_{||}}{q_s B}$ is the species gyroradius, and B is the equilibrium magnetic field strength. Field equations are solved with the PETSc library. The perturbed distribution function evolves as,

$$\frac{\partial\,\delta f}{\partial t} + \dot{\vec{X}}\cdot\frac{\partial\,\delta f}{\partial\vec{X}} + \dot{v}_{\|}\frac{\partial\,\delta f}{\partial v_{\|}} = -\dot{\vec{X}}_1\cdot\frac{\partial f_0}{\partial\vec{X}} - \dot{v}_{\|1}\frac{\partial f_0}{\partial v_{\|}}, \tag{8}$$

where the subscript 1 denotes the perturbed equations of motion, i.e. including only terms first order in ϕ and $A_{||}$. In this work, perturbed terms are dropped on the left-hand side, meaning simulations are inherently linear and cannot saturate. The distribution function is discretised with markers in the Klimontovich representation.

There are some key differences between ORB5[3] and XGC. ORB5 pushes markers and solves for the perturbed fields in magnetic coordinates except for an area near the axis. XGC pushes markers in polar coordinates, and solves for field perturbations on an unstructured, approximately field-following triangular mesh[20]. Parallel derivatives of field quantities in XGC are performed using finite differencing. The field-alignedness property of mesh nodes is improves accuracy of interpolation and derivatives in the parallel direction. It cannot be enforced over the entire area of the mesh; interpolation is otherwise performed between neighbouring nodes in barycentric coordinates.

ITG-KBM benchmark We perform a benchmark with drift-kinetic electrons as described in Section IV C of reference Ref.[19]. The geometry is Cyclone Base Case-like, with inverse aspect ratio $a/R_0 = 0.36$, axis magnetic

field strength is $B_0 = 2.0$ T and safety factor profile is $q(r) = 2.52(r/a)^2 - 0.16(r/a) + 0.86$.

The gradients are defined analytically by the equations

$$A/A(r_0) = \exp\left[-\kappa_A W_A \frac{a}{L_{ref}} \tanh\left(\frac{r - r_0}{W_A a}\right)\right] \quad (9)$$

and

$$L_{ref}/L_A = \kappa_A \cosh^{-2}\left(\frac{r - r_0}{W_A a}\right) \quad (10)$$

The profile of normalised plasma pressure, β, is varied by scaling the density. For this benchmark, $L_{ref} = R_0 = 1.67$ m, $\kappa_{Ti} = \kappa_{Te} = 6.96$, $W_{Ti} = W_{Te} = 0.3$; $\kappa_{ni} = \kappa_{ne} = 2.23$ and $W_{ni} = W_{ne} = 0.3$. The absolute values of the gradients are maximised at $r_0/a = 0.5$. We define β_{ref} as the normalised plasma pressure at this location. Temperature at this location is $T_{ref} = 2.14$ keV. The ions are deuterons. The simulated negative charge species has a mass twice that of physical electrons; the simulation m_i/m_e is equal to m_p/m_e.

The XGC mesh used has $\sim 1.9 \times 10^5$ nodes, with a minimum spacing at the gradient peak of ~ 2 mm, rising gradually to ~ 4 mm outside the region $0.15 < s < 0.6$. 2 mm corresponds to approximately half the thermal ion gyroradius around the peak gradient region. Nodes are placed on flux surfaces, with 248 surfaces in the range $0.0 < s < 1.0$. The number of nodes on each surface therefore varies, with the larger number of nodes per flux surface in the region $0.15 < s < 0.6$, where the mode is expected to be located. In this region, there are around 1000 nodes per surface, which is sufficient to resolve all poloidal modes permitted by the filter. Fourier filtering is applied to the fields at each solver step. In this case, all toroidal modes other than the desired $n = 19$ are filtered out. Poloidally, in XGC a filter is applied following the line of resonance $m_0 = qn$, with poloidal mode numbers outside the range $m_0 - 5 < m < m_0 + 5$ filtered out.

The toroidal gyrokinetic simulation domain is a 1/19th wedge of the tokamak. The gyrokinetic simulation toroidal grid resolution is therefore $N_{phi} = 16$. This would correspond to a hypothetical full-torus resolution of $N_{phi} = 304$. The computational cost of the gyrokinetic simulation does not scale with this full-torus resolution.

The XGC mesh is constructed with field-aligned nodes, the spacing dependent upon the full-torus angular separation of mesh planes, which here is $2\pi/304$ rad. This mesh generation toroidal resolution is used for determining node placement, and is not required to be equal to the toroidal resolution of the gyrokinetic simulation. The simulation is then performed in a 1/19 wedge of the tokamak, such that the field-alignedness property holds for a toroidal grid resolution of $N_{phi} = 16$. The $n = 1$ mode within the simulation domain therefore corresponds to the full-torus $n = 19$ mode.

Convergence To determine adequate numerical resolution for the benchmark with XGC, we perform convergence scans in particle number and timestep. The MV/PT version with Ohm's law predictor, in particular, permits poorly converged simulations with larger timesteps. The pure Hamiltonian scheme and the MV/PT formulation without Ohm's law predictor, on the other hand, tend to fail within a few timesteps if the simulation is not well converged in timestep. In Figure 1 (top), we test convergence in timestep for the MV/PT formulation with Ohm's law predictor. We use two different cases, one in which β_{ref} is close to the transition and another where it is deep in the KBM regime. In both cases, growth rates are well converged with a timestep of around 20 ns, whereas without the Ohm's law predictor a timestep of 4 ns is required for a functional simulation. Mode real frequencies, not shown, are approximately the same in all of these simulations, and therefore were not useful for testing convergence. In Figure 1 (bottom), we test convergence in numerical markers per grid triangle for the case deep in the KBM regime. The simulation is converged in growth rate at order 10 markers per cell.

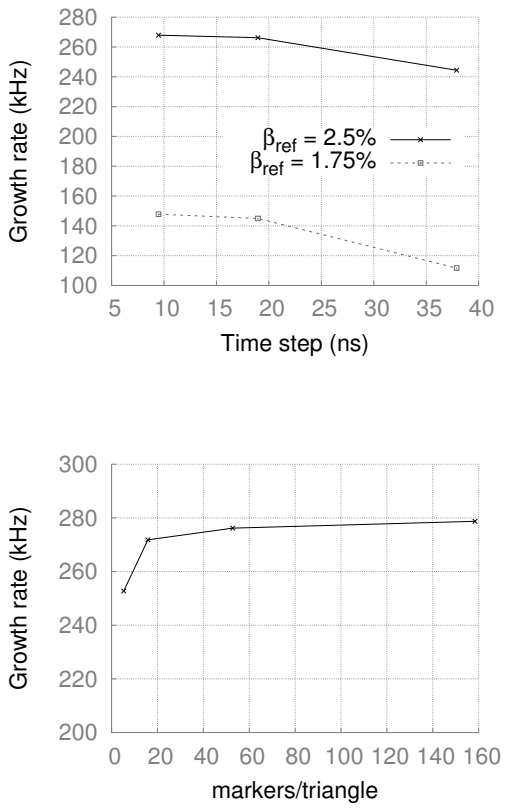

FIG. 1: Top, convergence of the full MV/PT scheme implemented in XGC in timestep for the $\beta_{ref} = 2.5\%$ and $\beta_{ref} = 1.75\%$ cases; bottom, convergence of the full MV/PT scheme implemented in XGC in marker number for the $\beta_{ref} = 2.5\%$ case with timestep ~ 19 ns.

Benchmark results The benchmark is run with XGC and ORB5. ORB5 has previously performed this bench-

mark with the electromagnetic gyrokinetic equations in the $p_{||}$ formulation[19], and here it is repeated with the mixed variables/pullback transformation scheme[3]. With XGC, the benchmark is performed with timestep $\Delta t \sim$ 19 ns and marker density $N_{ptl}/N_{tri} \sim 20$. Diagnostic quantities for comparison include the linear growth rate, real frequency, and mode structures at given parameters, and the location of the ITG-KBM transition in terms of β_{ref}. In figure 2 we show the linear growth rates and real frequencies calculated by XGC in comparison with the published results from the global version of GENE[19], and ORB5. The GENE growth rate and real frequency quantities are tabulated in Table V in Ref.[19]

As previously known, key physics features are the suppression of the toroidal ITG by finite β and possible dominance of KBM at higher β. The mode can be identified by its real frequency. The toroidal ITG is suppressed with increasing β_{ref} until the KBM becomes the fastest growing mode, identified by the sudden large increase in the real frequency. The KBM linear growth rate then increases rapidly with β_{ref} while real frequency decreases moderately. Good qualitative agreement is found between all the codes. Quantitative agreement is better between the two MV/PT-based particle-in-cell codes. The calculated transition point appears to be somewhat lower in β_{ref} using these two codes than the conventional continuum code GENE.

In figure 3 we show poloidal cross-sections calculated by XGC and ORB5 at zero toroidal angle of the electrostatic potential, ϕ, and parallel vector potential, $A_{||}$ calculated by XGC in the $\beta_{ref} = 0.5\%$ ITG case. Figure 4 shows the corresponding plots for the KBM at $\beta_{ref} = 2.5\%$ calculated by XGC and ORB5. In figure 5, the poloidally averaged squared electrostatic and paralle vector potentials are plotted, as calculated by XGC for the $\beta_{ref} = 1.3\%$ case. This can be compared with Fig. 12 b) and d) in Ref.[19] Characteristic spike structures are visible just below the critical β, which is an expected result of kinetic electron physics at the mode rational surfaces, where the electron evolution diverges most strongly from the adiabatic limit. Appearance of current sheets on the mode rational surfaces can be noticed from the $A_{||}$ spikes, which have a stablising effect on the ITG mode.

Conclusion In this paper we report on the implementation in the XGC code[11] of the mixed variables/pullback transformation (MV/PT) formulation[4] of the electromagnetic gyrokinetic equations[1] for simulation of high temperature magnetic confinement fusion plasmas. This technique involves a variable splitting of the parallel vector potential between symplectic and Hamiltonian parts. Pullback transformation is then performed as part of the numerical scheme to accumulate the parallel vector potential in the relatively benign symplectic component. An Ohm's law predictor can optionally be used to estimate some remaining component of the Hamiltonian part of the parallel vector potential, and to simplify the weight evolution equation by an analytical cancellation of a generally large term.

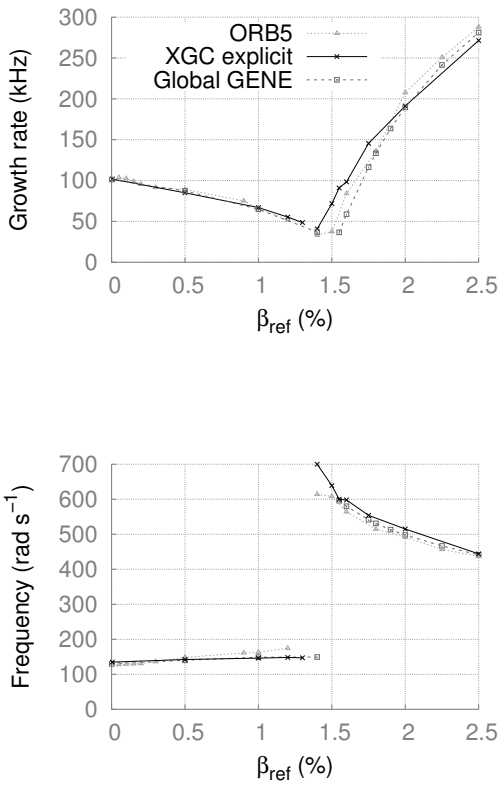

FIG. 2: Comparison of the growth rates and real mode frequencies calculated by the XGC and ORB5 mixed variables/pullback explicit electromagnetic implementations, and the continuum GENE global version for a range of reference position beta values in the CYCLONE-like case.

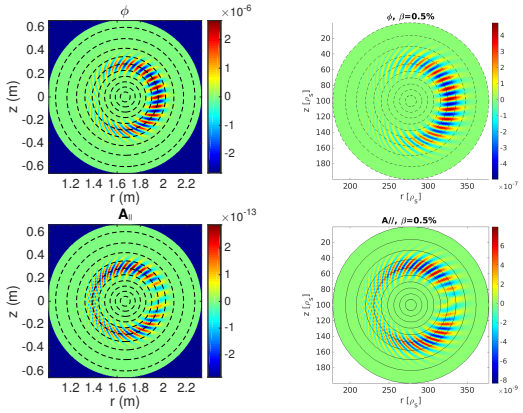

FIG. 3: Poloidal cross-sections of the perturbed electrostatic (top) and parallel vector (bottom) potentials as calculated with XGC (left) and ORB5 (right) for the ITG mode at $\beta = 0.5\%$. In these linear simulations, ϕ and $A_{||}$ units are arbitrary.

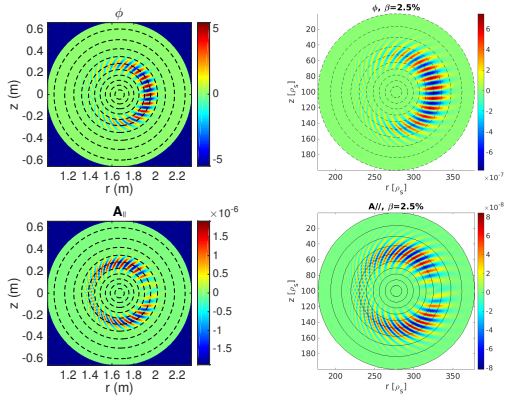

FIG. 4: Poloidal cross-sections of the perturbed electrostatic (top) and parallel vector (bottom) potentials as calculated with XGC (left) and ORB5 (right) for the KBM mode at $\beta = 2.5\%$. In these linear simulations, ϕ and $A_{||}$ units are arbitrary.

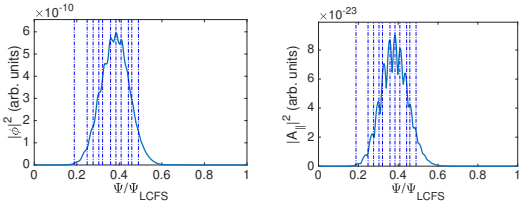

FIG. 5: Poloidally averaged squared perturbed electrostatic (left) and parallel vector (right) potentials as calculated by XGC for the $\beta_{ref} = 1.3\%$ ITG case. Dashed lines represent, from left to right, the rational surfaces at $q = \frac{11}{10}, \frac{6}{5}, \frac{5}{4}, \frac{13}{10}, \frac{4}{3}, \frac{7}{5}, \frac{29}{20}, \frac{3}{2}, \frac{11}{7}, \frac{8}{5}, \frac{5}{3}$.

This implementation had also previously been introduced in the ORB5 code[3]. In this paper, we report results of a standard benchmark case performed with the MV/PT formulation by XGC and ORB5[19]. Results for this benchmark from ORB5 with a Hamiltonian formulation were previously reported in the literature; the MV/PT results are reported here for the first time. The benchmark tests the transition from the electrostatic ion temperature gradient-driven mode regime to the kinetic ballooning mode regime in a standard aspect ratio $R_0/a_0 \sim 3.0$) circular tokamak with experimentally relevant plasma profiles. Relevant benchmark quantities are the growth rates, real frequencies and eigenstructures of the dominant mode at different values of the normalised plasma pressure (β), varied by scaling the density profile. Another relevant benchmark quantity is the location of the transition region in β.

Good agreement is found in growth rate and real frequency between XGC and ORB5 using the MV/PT formulation, and between both codes and the continuum gyrokinetic code GENE (whose formulation is described in detailed publications[7,21]); GENE results are tabulated in the literature[19]. This comparison is the most comprehensive to be published and with the most challenging and physically relevant comparison case for the MV/PT formulation. It gives confidence in the correctness of the explicit electromagnetic implementation in the XGC code and the applicability of the MV/PT approach to electromagnetic gyrokinetic PIC simulation.

The non-linear form[4] of the MV/PT scheme has been implemented for XGC and turbulence simulations attempted[22–24]. The scheme is compatible with XGC's total-f capability[11]. Electromagnetic gyrokinetic simulations of the whole tokamak are in sight. Resolving low toroidal mode number modes will be important and has been challenging in the past; the MV/PT scheme has simulated the linear $n = 1$ internal kink mode in tokamak geometry[3], and the nonlinear collisionless tearing mode in slab geometry[4].

ACKNOWLEDGMENTS

The authors would like to thank J. Dominski, R. Hager and S. Ku for useful discussions. The authors gratefully acknowledge the support of A. Bhattacharjee and S. Hudson, and P. Helander for facilitating exchanges in connection with this work. This work is supported by US Department of Enegy Office of Science, through SciDAC-4 and base theory program, under Contract Number DE-AC02-09CH11466. This research used resources of the National Energy Research Scientific Computing Center (NERSC), a U.S. Department of Energy Office of Science User Facility operated under Contract No. DE-AC02-05CH11231. Raw data were generated at this facility. Derived data supporting the findings of this study are available from the corresponding author upon reasonable request. The United States Government retains and the publisher, by accepting the article for publication, acknowledges that the United States Government retains a non-exclusive, paid-up, irrevocable, world-wide license to publish or reproduce the published form of this manuscript, or allow others to do so, for United States Government purposes.

[1] A. J. Brizard and T. S. Hahm, Rev. Mod. Phys. **79**, 421 (2007).
[2] E.Lanti, N.Ohana, N. Tronko, T. Hayward-Schneider, A. Bottino, B. F. McMillan, and A. Mishchenko, Comput. Phys. Commun. **251**, 107072 (2020).
[3] A. Mishchenko, A. Bottino, A. Biancalani, R. Hatzky, T. Hayward-Schneider, N. Ohana, and E. Lanti, Comput. Phys. Commun. **238**, 194 (2019).
[4] R. Kleiber, R. Hatzky, A. Könies, A. Mishchenko, and E. Sonnendrücker, Phys. Plasmas **23**, 032501 (2016).
[5] V. Kornilov, R. Kleiber, R. Hatzky, L. Villard, and G. Jost, Phys. Plasmas **11**, 3196 (2004).
[6] Y. Chen and S. Parker, J. Comput. Phys. **220** (2007).
[7] T. Görler, X. Lapillonne, S. Brunner, T. Dannert, F. Jenko, F.Merz, and D.Told, J. Comput. Phys. **251**, 107072 (2010).
[8] A. Peeters, Y. Camenen, F. J. Casson, W. Hornsby, A. Snodin, D. Strintzi, and G. Szepesi, Comput. Phys. Commun. **180**, 2650 (2009).
[9] C. Chang, S. Ku, G. Tynan, R. Hager, R. Churchill, I. Cziegler, M. Greenwald, A. Hubbard, and J. Hughes, Phys. Rev. Lett. **118**, 175001 (2017).
[10] S. H. Ku, R. Hager, C. S. Chang, J. Kwon, and S. Parker, J. Comp. Physics **315**, 467 (2015).

[11]S. Ku, C. S. Chang, R. Hager, R. M. Churchill, G. R. Tynan, I. Cziegler, M. Greenwald, J. Hughes, S. E. Parker, M. F. Adams, E. D'Azevedo, and P. Worley, Phys. Plasmas **25**, 056107 (2018).
[12]T. Moritaka, R. Hager, M. D. J. Cole, S. Lazerson, C. S. Chang, S. H. Ku, S. Matsuoka, S. Satake, and S. Ishiguro, Plasma **2(2)**, 179 (2019).
[13]M. D. J. Cole, R. Hager, T. Moritaka, J. Dominski, R. Kleiber, S. Ku, S. Lazerson, J. Riemann, and C. S. Chang, Phys. Plasmas **26**, 082501 (2019).
[14]M. D. J. Cole, T. Moritaka, R. Hager, J. Dominski, S. Ku, and C. S. Chang, Phys. Plasmas **27**, 044501 (2020).
[15]R. Hager, J. Lang, C. S. Chang, S. Ku, Y. Chen, S. E. Parker, and M. F. Adams, Phys. Plasmas **24**, 054508 (2017).
[16]B. Sturdevant and et al., (In preparation for submission to Phys. Plasmas).
[17]A. Mishchenko, M. D. J. Cole, R. Kleiber, and A. Könies, Phys. Plasmas **24**, 052113 (2014).
[18]A. Mishchenko, A. Könies, R. Kleiber, and M. D. J. Cole, Phys. Plasmas **21**, 092110 (2014).
[19]T. Görler, N. Tronko, W. A. Hornsby, A. Bottino, R. Kleiber, C. Norscini, V. Grandgirard, F. Jenko, , and E. Sonnendrücker, Phys. Plasmas **23**, 072503 (2016).
[20]F. Zhang, R. Hager, S.-H. Ku, C. S. Chang, S. C. Jardin, N. M. F. nad E. S. Seol, E. Yoon, and M. Shephard, Eng. Comput. **32**, 285 (2016).
[21]N. Tronko, A. Bottino, T. Görler, E. Sonnendrücker, D. Told, and L. Villard, Phys. Plasmas **24**, 056115 (2017).
[22]S. Ku, R. Hager, M. D. J. Cole, A. Y. Sharma, A. Mishchenko, and C. S. Chang, Bull. American Phys. Soc. **62nd Annual Meeting of the APS Division of Plasma Physics**, JP20.00009 (2020).
[23]R. Hager, S. Ku, M. D. J. Cole, A. Sharma, A. Mishchenko, and C. Chang, Bull. American Phys. Soc. **62nd Annual Meeting of the APS Division of Plasma Physics**, VP14.00021 (2020).
[24]A. Y. Sharma, M. D. J. Cole, B. J. Sturdevant, A. Mishchenko, S. Ku, R. Hager, C. S. Chang, W. Guttenfelder, and S. M. Kaye, Bull. American Phys. Soc. **62nd Annual Meeting of the APS Division of Plasma Physics**, VP14.00024 (2020).